

Quantifying Uncertainty due to Imperfect Force Prediction Models: A General Methodology with Applications to Fluid Drag Loads

Tina Kashef and Steven R. Winterstein
Civil Eng. Dept., Stanford University
Stanford, CA, USA

Rune Torhaug
Det Norske Veritas
Høvik, Norway

Abstract

Various methods are presented here to characterize uncertainty due to imperfect force prediction models. These use different statistical approaches to systematically compare “true” and predicted load levels. In particular, the reporting of marginal error statistics (e.g., mean bias and uncertainty) is shown to generally be insufficient to recover the marginal distribution of applied loads, as required for reliability analysis and design. Methods are shown to address this insufficiency, through regression-based analysis and comparison of ordered loads data. While results here specifically consider fluid drag loads, the methods are intended to have wider applications; e.g., to statistically compare actual wave heights with those based on hindcast methods.

Introduction

One of the main steps in the design of offshore platforms—and almost all other structures as well—is estimating an appropriate extreme force which the structure needs to be designed to withstand. This force is commonly chosen to be the force which is exceeded with a certain probability or return period, e.g., the 100-year force level. A load factor is then applied to this force, to cover (1) natural randomness in the ocean wave process, and (2) uncertainty associated with our imperfect models of the loads given the waves.

In this paper we focus on the second step, i.e., studying force estimates associated with extreme waves, and their associated uncertainty. We show a range of methods to characterize this uncertainty, based on statistical comparison of “true” and predicted load levels. In this paper, “true” loads are estimated by time-domain simulation, and compared with simpler design wave predictions. The methodology is general, however, and can equally well be used with actual measured load data. It can also be applied to characterize other sources of model uncertainty; e.g., by statistically comparing actual and hindcast wave heights.

Design Wave Approach

For quasi-static structures such as jackets, the largest force during a given seastate is typically assumed to be caused by the largest wave. Frequently, the actual wave elevation time history during this largest wave is approximated with a “design wave”, which is then used to calculate the response. The “design wave” is a wave with a selected profile which matches a number of the parameters of the largest wave, such as its amplitude and period. This approximation of the water elevation results in a deviation from the full time-history analysis which is due to the following two factors:

1. Approximating the actual irregular water surface with a smooth, deterministic wave profile. This mainly affects the concurrent elevation at different piles.
2. Approximating the resulting kinematics of the irregular waves with those of the smooth profile.

The design wave method includes the following steps:

1. Specifying the wave parameters. These typically include the amplitude and period, but may also include other parameters such as steepness, water depth, etc. Two common choices for the wave amplitude are the crest height and half the wave height of the wave to be modeled. The wave period can be set to the period of the modeled wave, or it can be estimated from the peak spectral period of the waves. We compare all these choices and present the results in the following sections.
2. Choosing a wave profile which allows the parameters above to be matched. Common choices include the linear (sinusoidal) profile, higher-order profiles (e.g., Stokes 5th order), and the wave autocorrelation function (e.g., Tromans et al, 1991). In this paper we compare the autocorrelation and sinusoidal profiles.
3. Choosing the kinematics and force models. The kinematics model is used to find the water velocity profile from the wave elevation profile, and the force model is used to calculate the local loads on the members due to the water velocity. In our calculations we use linear kinematics to calculate the water particle

velocity up to the mean water level. We then stretch the results to the actual free surface using Wheeler stretching. We use the drag term of the Morison force model to find the local forces on the members (e.g., Sarpkaya and Isaacson, 1981). For each of the structures studied, we finally estimate the total base shear from an idealized structural model consisting of one or more piles. (Note that the same kinematics and force models are used both in the time-domain simulation and in the design wave estimation. For our purposes, then, Morison’s equation is considered exact. Hence, as noted above, differences result only from the replacement of the actual irregular wave surface with an idealized wave profile.)

In addition to the model parameters, the accuracy of the results may also depend on the characteristics of the structure (e.g., the number of piles and their distances) and the wave being modeled (e.g., the response to every single wave cycle or only the response to the largest wave). In this paper we study a number of different structures and seastates, as well as two different wave populations: the largest 2% waves in the seastate, and the single largest wave in the one-hour seastate. The first population—the largest 2%—is chosen to mimic the Ocean Test Structure (OTS) study, on which the API design guidelines are partially based. The second—the single largest wave—relates more directly to the design problem, as well as perhaps containing a more homogeneous population of extreme wave cycles.

OTS Model and Background

The first model we study is based on the Ocean Test Structure (OTS). The OTS was a $20 \times 40 \times 120$ ft jacket structure which was located in the Gulf of Mexico in 66 feet of water depth between November 1976 and June 1978 (Haring and Spencer, 1979). Total base shear and overturning moment on the platform were measured using calibrated sensors. Individual wave events that were among the largest 2% of zero-crossing wave heights in each seastate and created a post-critical flow regime during wave crest passage were selected for further study. A large majority of this data was obtained during two winter storms and hurricane Anita. Table 1 shows the characteristics of each of these storms.

In subsequent studies, measured responses of the structure were compared with the results of corresponding wave force predictions (Haring et al, 1979; Heideman and Weaver, 1992). These studies found a relatively small bias in the predictions. However, the ratio of the predicted to measured forces was found to have an average coefficient of variation (ratio of standard deviation to mean) of 25%. As noted above, these results are part of the basis for standard probabilistic analysis and LRFD codes for shallow-water jacket structures (API, 1993).

In this study we use a simplified structural model for the OTS which consists of 2 piles set 14 meters apart, with a water depth of 22 meters. Each pile is intended to represent the equivalent of two (of the four) legs of the jacket structure. The seastate modeled is a winter storm with significant wave height $H_S = 5.5$ meters and peak spectral period $T_P = 7.5$ seconds—a somewhat higher significant wave height than the OTS structure was subjected to. We compare the total base shear for a variety of cases. First, we select the largest 2% of the waves in 12 individual simulated storms lasting 1 hour each, i.e, 165 waves in total, and study the effect of the choice of wave profile (i.e., sinusoidal vs. autocor-

relation) and defining wave characteristic (i.e., wave height vs. crest) on the accuracy of the predictions. We then move on to study global hourly wave and force maxima in 75 hours of waves simulated from the same seastate.

OTS Results 1: Bias-Corrected Error Statistics

The predicted values will not, in general, coincide with the actual values produced by the simulation model. In fact, even the average (“expected”) values of the two may not coincide, i.e., the predictions may be *biased*. For example, we may expect that simple sinusoids may yield lower force levels than higher-order Stokes profiles, and that the autocorrelation profile (with its shallower trough) may yield still lower forces. These differences can be corrected by introducing a *bias correction factor* B which, when multiplied by the original predictor F_p , produces an unbiased predictor F_u . In other words:

$$F_u = B \cdot F_p ; \quad B = E[F_t]/E[F_p] \quad (1)$$

Here $E[\cdot]$ denotes the expected value of the bracketed term. F_u is hence referred to as the *bias-adjusted* (or *unbiased*) prediction. The difference between the true force, F_t , and the bias-adjusted prediction, F_u , will now be a mean-zero random error term ϵ , i.e.,

$$\epsilon = F_t - F_u = F_t - B \cdot F_p \quad (2)$$

The error term ϵ represents that part of the variations in F_t that our (bias-adjusted) model does not capture. Thus, its variance, σ_ϵ^2 , reflects the remaining variability in F_t when F_p is known. In order for the bias-adjusted prediction to be a good estimator of F_t , this remaining variability should be small compared to the original variability in F_t . One useful way to report σ_ϵ^2 , therefore, is to normalize it by the variance $\sigma_{F_t}^2$ of the true forces. In particular, we can quantify the estimating power of our model through the *coefficient of determination* R_{F_t, F_p}^2 , defined as

$$R_{F_t, F_p}^2 = 1 - \left[\frac{\sigma_\epsilon}{\sigma_{F_t}} \right]^2 \quad (3)$$

i.e., the percentage of the variance in F_t that is explained by the bias-adjusted model.

An alternative way to normalize σ_ϵ is to divide by the mean force level $E[F_t]$, which characterizes both the true forces and their bias-adjusted predictions. This leads, roughly speaking, to a quantity analogous to a coefficient of variation, and is hence denoted here by COV:

$$\text{COV} = \frac{\sigma_\epsilon}{E[F_t]} \quad (4)$$

Because R^2 and COV are simply different normalized versions of σ_ϵ , they are directly related; i.e.,

$$\text{COV} = \frac{\sigma_\epsilon}{E[F_t]} = \frac{\sigma_\epsilon}{\sigma_{F_t}} \cdot \frac{\sigma_{F_t}}{E[F_t]} = \sqrt{1 - R_{F_t, F_p}^2} \cdot V_{F_t} \quad (5)$$

in which V_{F_t} is the coefficient of variation of the true force levels. (The last equality uses Eq. 3.) Again, better predictive models lead to higher R^2 values, and hence more greatly reduce the COV value from its original level, V_{F_t} . The numerical values of R_{F_t, F_p}^2

Storm	Significant Wave Height (m)	Direction	Duration (hrs)
March 28, '77	3.5	SE	7
Hurricane Anita	3.5	SSE	24
Jan 25, '78	4.5	SW	13

Table 1: Three major storms affecting the OTS model.

and/or COV clearly depend on the characteristics of our predictive model. Thus we can use these values to compare the predictive power of different models, as well as to compare how different cases—such as different structures and wave populations—affect the accuracy of the predictions.

We first study the response to the 2% largest waves (as in the original OTS test case). We look at models that use either an autocorrelation or a sinusoidal profile, and either the wave crest or half the wave height as the amplitude. In the case of the sinusoidal profile, which can match the wave period as well, we use the exact period of the modeled wave. Table 2 shows the results of these comparisons. The remaining COV level in all cases is seen to be about 25%-30%. These values are very close to the original OTS studies, which reported a remaining COV of 25% (Haring and Spencer, 1979). Notably, our simulated results appear to roughly reproduce the variability found in the original test data. Thus, it appears possible that the design wave definition can introduce a realistic amount of load variability, even if Morison’s equation is assumed to be exact. In addition, we can see that none of these bias-adjusted models are able to reduce the original COV of 36% considerably.

OTS Results 2: Predicting Marginal Force Distributions

For reliability calculations, we need to estimate not only marginal statistics of the error, ϵ , but also the resulting marginal distribution of F_t (or at least some measure of the variance of F_t). Formally, F_t is recovered from F_p and ϵ as in Eq. 2:

$$F_t = B \cdot F_p + \epsilon \quad (6)$$

To estimate marginal statistics of F_t from Eq. 6, we can construct a new sample of F_t by adding an error term to each bias-adjusted estimate $B \cdot F_p$. Assuming ϵ is independent of F_p , this error term can be chosen at random from the vector of error values associated with the bias-adjusted predictions. Thus, with each random assignment of errors, we can calculate a new estimate $\hat{\sigma}_{F_t}$ for σ_{F_t} . If this exercise is repeated many times, $E[\hat{\sigma}_{F_t}]$ should be equal to the original value of σ_{F_t} . To test this error-resampling approach, we have created 10,000 new samples for F_t . The results obtained for $E[\hat{\sigma}_{F_t}]$, normalized by $E[F_t]$, are the “Error resampled V_{F_t} ” values in Table 3.

Apart from bootstrapping, σ_{F_t} can also be calculated directly using the relationship $F_t = B \cdot F_p + \epsilon$ from Eq. 6. Calculating the variances of both sides,

$$\sigma_{F_t}^2 = B^2 \cdot \sigma_{F_p}^2 + \sigma_\epsilon^2 + 2B \cdot \rho_{F_p, \epsilon} \cdot \sigma_{F_p} \cdot \sigma_\epsilon \quad (7)$$

in which $\rho_{F_p, \epsilon}$ is the correlation coefficient between F_p and ϵ . Assuming independent errors ($\rho_{F_p, \epsilon} = 0$) and dividing by $E^2[F_t]$

yields

$$V_{F_t}^2 = B^2 \cdot V_{F_p}^2 + \text{COV}^2 \quad (8)$$

The results for this approach are also reflected in Table 3. As expected, these are equivalent (within numerical noise) to the error-resampling results, because both assume independence. More notably, in the case of predictions using crest height, the assumption of independent errors is shown to be significantly in error. In particular, it leads here to *overestimation* of the actual marginal COV, V_{F_t} . This indicates that for these predictions (based on crest heights), a negative correlation must exist between F_p and ϵ . In contrast, the assumption of independent errors appears fairly accurate for predictions based on wave heights. A plot of ϵ versus F_p for both cases—as seen in Figures 1 and 2—confirms this conclusion.

Perhaps the most important point is that it is generally insufficient to only report marginal statistics of the error ϵ (though this is commonly done). In general we also need information regarding the correlation between the errors and predicted values. Once we take this correlation into account, we can use either of the approaches above to estimate V_{F_t} . The error-resampling method can be modified such that random error terms are drawn only from a local pool (occurring for F_p values close to the one considered). For our example, this modified method produces an estimate of 0.36 for V_{F_t} , the same as the original V_{F_t} value. Similarly, if we substitute the observed correlation value $\rho_{F_p, \epsilon} = -0.47$ in Equation 7, it also yields the original value 0.36 for V_{F_p} as expected.

OTS Results 3: Regression-Based Results

By its definition, Eq. 6 defines a trend line, $F_t = B F_p$, that passes through the origin ($F_t = F_p = 0$). In our previous example of predictions using crest height, the resulting error was found to be negatively correlated with F_p . This indicates that for small values of F_p the error is most often positive, i.e., F_t lies above the model line, whereas for large values of F_p the error is most often negative, i.e., F_t lies below the modeled line. This point is illustrated in Figure 3.

Figure 3 suggests that one may achieve uncorrelated errors by using a calibration model that allows for an intercept (positive in this example). Mathematically, this model can be expressed as:

$$F_t = \alpha + \beta F_p + \epsilon \quad (9)$$

The two parameters α and β can be chosen such that the model satisfies two constraints: (1) unbiased estimations of F_t , and (2) errors that are uncorrelated with F_p . Note that only the first constraint was satisfied in the bias-adjustment model. The two

Profile	Matching Crest	Matching Height
Sinusoid	$R_{F_t, F_p}^2 = 0.47$	$R_{F_t, F_p}^2 = 0.56$
Period: T_{ex}	COV=0.27	COV=0.24
Autocorrelation	$R_{F_t, F_p}^2 = 0.41$	$R_{F_t, F_p}^2 = 0.40$
	COV=0.28	COV=0.28

Table 2: Results for error standard deviations, σ_ϵ , normalized to report the quantities COV (Equation 4) and R_{F_t, F_p}^2 (Equation 3). Results apply to OTS model simulations, 2% largest waves. Note also that the original COV of F_t is 36%. It appears that none of these bias-adjusted models is able to reduce this original COV considerably.

	Matching Crest	Matching Height
V_{F_t}	0.36	0.36
V_{F_p}	0.36	0.26
COV	0.27	0.24
$\sqrt{(V_{F_u}^2 + \text{COV}^2)}$	0.45	0.36
Error-resampled V_{F_T}	0.45	0.35

Table 3: Actual results for V_{F_t} versus two predictions of V_{F_t} that assume independent errors ϵ . Predictions (Eq. 8 and independent “Error-resampling”) should be identical; differences are due only to numerical noise. Again, results apply to OTS model simulations, upper 2% largest waves.

constraints can be expressed mathematically in the following form:

$$E[F_t] = E[\alpha + \beta \cdot F_p] = \alpha + \beta \cdot E[F_p] \quad (10)$$

and

$$\text{Cov}[\epsilon, F_p] = 0 \quad (11)$$

Here $\text{Cov}[\epsilon, F_p]$ denotes the covariance between the two bracketed terms. (This should be distinguished from the upper-case “COV” notation, which as noted is an acronym for the coefficient of variation.) Substituting for ϵ from Equation 9,

$$\begin{aligned} \text{Cov}[\epsilon, F_p] &= \text{Cov}[F_t - \alpha - \beta F_p, F_p] \\ &= \text{Cov}[F_t, F_p] - \beta \text{Cov}[F_p, F_p] \end{aligned} \quad (12)$$

Setting this quantity to zero, the required β is

$$\beta = \frac{\sigma_{F_t, F_p}}{\sigma_{F_p}^2} \quad (13)$$

The parameter α can finally be found from Equation 10:

$$\alpha = E[F_t] - \frac{\sigma_{F_t, F_p}}{\sigma_{F_p}^2} E[F_p] \quad (14)$$

These results for α and β are identical to those found in linear regression theory. Hence the current model also provides a least-square-error linear estimator of F_t , i.e., among all estimators of the form $\alpha + \beta \cdot F_p$, the parameters found in Equations 13 and 14 result in an estimate that has the least squared error. Note, of course, that while the errors in this model are uncorrelated with F_p , they are not necessarily independent of it.

We now return to our comparison of prediction models. For each of the four cases studied above, the R^2 and COV values (for estimates calibrated by linear regression) are reported in Table 4. The R^2 and COV values reported for crest-based predictions show a notable improvement compared to the bias-adjustment results. Because errors are now ensured to be uncorrelated, these summary statistics provide a more descriptive picture of the performance

of these predictors. For example, the crest-based sinusoidal predictor can now truly be said to explain 58% of the variability of F_t . (R_{F_t, F_p} can now accurately be called the coefficient of determination between F_t , and F_p)

The clearest trend in these results is the general superiority of using the sinusoidal profile, when calibrated to preserve the exact period T_{ex} of the extreme wave being modeled. As this knowledge will not generally be available, Table 5 shows amended results in which this sinusoidal profile is now used with a single period representative of the seastate—the peak spectral period T_p . Now we find that when the sinusoidal and autocorrelation profiles are calibrated with the same information—whether crest or total wave height—they show identical predictive ability. This is a common finding throughout our work: the precise choice of profile shape has little or no impact on our force prediction ability. (Of course, the choice of profile will typically affect our mean force predictions, and hence the degree of bias that may exist. This is also true for the choice of representative period: using periods slightly shorter than T_p affects the bias, but not the predictive ability.)

Because our “true” forces in fact are simulated using Morison’s equation, it may appear somewhat surprising that a design wave approach can explain only 40–48% of their observed variability. Several factors might be advanced to explain this: (1) the selection of the upper 2% waves, rather than only the most extreme in the hourly storm; and (2) the relatively wide spacing of the OTS model, and hence its relatively broad spatial sampling of the sea surface. We first study item (1), by considering predictions of only the largest force in each (simulated) one-hour storm. Table 6 shows the corresponding results. As might be expected, because we are dealing with a narrower set of extreme waves/forces, all COVs are lower. Indeed, the original COV of F_t is only 0.19. As far as their relative predictive power, however, the gains of considering only hourly maxima are modest: crest-based predictions now explain 57%, while height-based models explain 46%. The remaining question, concerning leg spacing, we address below by

Profile	Matching Crest	Matching Height
Sinusoid	$R_{F_t, F_p}^2=0.58$	$R_{F_t, F_p}^2=0.56$
Period: T_{ϵ_x}	COV=0.24	COV=0.24
Autocorrelation	$R_{F_t, F_p}^2=0.48$ COV=0.26	$R_{F_t, F_p}^2=0.40$ COV=0.28

Table 4: Results for error standard deviations, σ_ϵ , normalized to give COV (Equation 4) and R_{F_t, F_p}^2 (Equation 3). Results apply to OTS model simulations calibrated using linear regression.

Profile	Matching Crest	Matching Height
Sinusoid	$R_{F_t, F_p}^2=0.48$	$R_{F_t, F_p}^2=0.40$
Period: T_p	COV=0.26	COV=0.28
Autocorrelation	$R_{F_t, F_p}^2=0.48$ COV=0.26	$R_{F_t, F_p}^2=0.40$ COV=0.28

Table 5: Regression results for COV and R_{F_t, F_p}^2 , now comparing predictions each with one parameter only (crest or total wave height).

Profile	Matching Crest	Matching Height
Sinusoid	$R_{F_t, F_p}^2=0.57$	$R_{F_t, F_p}^2=0.46$
Period: T_p	COV=0.12	COV=0.14
Autocorrelation	$R_{F_t, F_p}^2=0.57$ COV=0.12	$R_{F_t, F_p}^2=0.46$ COV=0.14

Table 6: Regression results for COV and R_{F_t, F_p}^2 for predictions of hourly extremes (rather than upper 2% waves). In this case, original COV of F_t is 0.19.

considering more realistic, North Sea jacket geometries.

North Sea Results

We now simulate storms typical of 100-year North Sea conditions: $H_S=15.5\text{m}$ and $T_P=16.5\text{s}$. Focusing only on global hourly wave and response maxima from 75 hours of simulated waves, we study the effect of column spacing—in particular, we study a single-pile model, a two-pile model with 25 meter leg spacing, and a two-pile model with 68 meter leg spacing. The 25 meter leg spacing is fairly typical of our jacket (water depth=70m), while the 68 meter leg spacing is chosen to mimic the wide leg spacing (as compared to wave length) of the OTS structure.

Table 7 shows results from regression analysis for the OTS-like case (leg spacing=68m). The crest-based predictions show results similar to those obtained for the OTS structure. The predictions using wave height, however, have much higher R^2 values than found for the OTS structure. As a result, wave height performs better than crest height for this structure. Because wave height reflects characteristics between crest and subsequent trough, it perhaps is most useful in cases (such as these) of unusually wide leg spacing.

To address this, Table 8 shows corresponding results as a function of leg spacing. The change in results is dramatic: for 1 pile and even for 2 closely spaced piles, crest-based predictions increase greatly in accuracy. This is physically sensible, since traditional, drag-dominated jackets are most sensitive to the crest height, at whose arrival the extreme base shear generally occurs. Because the total wave height does not carry this extreme crest informa-

tion, its predictive ability does not grow as leg spacing decreases.

This is a finding whose accuracy, of course, is limited here by our use of simulated (rather than actual) wave forces. Nonetheless, as a general matter it suggests that force modeling uncertainty may depend critically on the representativeness of both the structure (e.g. leg spacing) and the extreme wave population (e.g., hourly extremes vs upper 2%). This suggests that it may be useful to apply these approaches to actual wave force data, in order to better quantify appropriate COV levels. Focus on more extreme waves and more representative structures would help to quantify this. It also suggests that crest-based predictions should be considered as viable alternatives to the traditional predictions based on total wave height.

Conclusions

- We have first performed time-domain simulations that sought to mimic the OTS measurements by preserving its geometry and its focus on the upper 2% extreme waves. We have focused on statistics of the error, ϵ , between true (simulated) and design-wave predictions. Using a bias-adjusted model, we find error statistics similar to those reported from OTS; e.g., COV values of the order of 25% (Table 2).
- We find it generally insufficient—and sometimes misleading—to report only marginal statistics of ϵ . Specifically, there may be correlations between ϵ and predicted forces F_p that also need to be considered. One solution to this is to identify errors through regression, thereby ensuring they remain uncorrelated with F_p .

Profile	Matching Crest	Matching Height
Sinusoid	$R_{F_t, F_p}^2=0.55$	$R_{F_t, F_p}^2=0.68$
Period: T_p	COV=0.14	COV=0.11
Autocorrelation	$R_{F_t, F_p}^2=0.55$	$R_{F_t, F_p}^2=0.68$
	COV=0.14	COV=0.11

Table 7: Regression results for COV and R_{F_t, F_p}^2 , North Sea hourly extremes, jacket leg spacing=68m. In this case, original COV of F_t is 0.20.

Leg Spacing	COV of F_t	Matching Crest	Matching Height
68 m	0.20	$R_{F_t, F_p}^2=0.55$ COV=0.14	$R_{F_t, F_p}^2=0.68$ COV=0.11
25 m	0.22	$R_{F_t, F_p}^2=0.80$ COV=0.10	$R_{F_t, F_p}^2=0.66$ COV=0.13
Single Pile	0.23	$R_{F_t, F_p}^2=0.95$ COV=0.05	$R_{F_t, F_p}^2=0.63$ COV=0.14

Table 8: Regression results for COV and R_{F_t, F_p}^2 , North Sea hourly extremes, various leg spacings.

- Using regression to define R^2 , the amount of variability explained by our predictor, we have analyzed a number of cases. In cases of unusually wide leg spacing (OTS and a similarly scaled North Sea jacket), various predictors are found to explain no more than 50–60% of the observed variability in base shear. Effective COV levels reduce nonetheless—e.g., to about 10–15%—when our wave population is limited to the hourly extreme (rather than the upper 2%). The most dramatic change, however, comes when the leg spacing is reduced to more realistic levels: crest-based predictions increase greatly in accuracy. This suggests that crest-based predictions should be considered as viable alternatives to traditional predictions, which are based on total wave height.
- Force modeling uncertainty may depend critically on the representativeness of both the structure (e.g. leg spacing) and the extreme wave population (e.g., hourly extremes vs upper 2%). This suggests that it may be useful to apply these approaches to actual wave force data, in order to better quantify appropriate COV levels. Focus on more extreme waves, and more representative structures, would help to quantify this.
- In all cases when regression was used to define modeling errors, sinusoidal profiles (matched to T_p) and autocorrelation profiles are virtually identical in terms of their predictive power. The choice of profile appears, therefore, to have little effect on these predictions—except, of course, in terms of mean force levels and potential biases.

- Haring, R.E., O.A. Olsen, and P. I. Johansson (1979). Total wave force and moment vs design practice. *Proc., Intl. Conf. on Civ. Eng. in the Oceans IV, ASCE*, 805–819.
- Heideman, J.C. and T.O. Weaver (1992). Static wave force procedure for platform design. *Proc., Intl. Conf. on Civ. Eng. in the Oceans V, ASCE*, 496–517.
- Sarpkaya, T. and M. Isaacson (1981). *Mechanics of wave forces on offshore structures*, Von Nostrand Reinhold.
- Tromans, P.S., A.H.R. Anatrak, and P. Hagemeyer (1991). New model for the kinematics of large ocean waves application as a design wave. *Proc., 1st Intl. Offshore and Polar Eng. Conf., ISOPE*, 64–71.

REFERENCES

- API, RP2A-LRFD (1993). *Recommended practice for planning, designing and constructing fixed offshore platforms—load and resistance factor design*, 1st edition, American Petroleum Institute.
- Haring, R.E. and L.P. Spencer (1979). Ocean test structure data base. *Proc., Intl. Conf. on Civ. Eng. in the Oceans IV, ASCE*, 669–683.

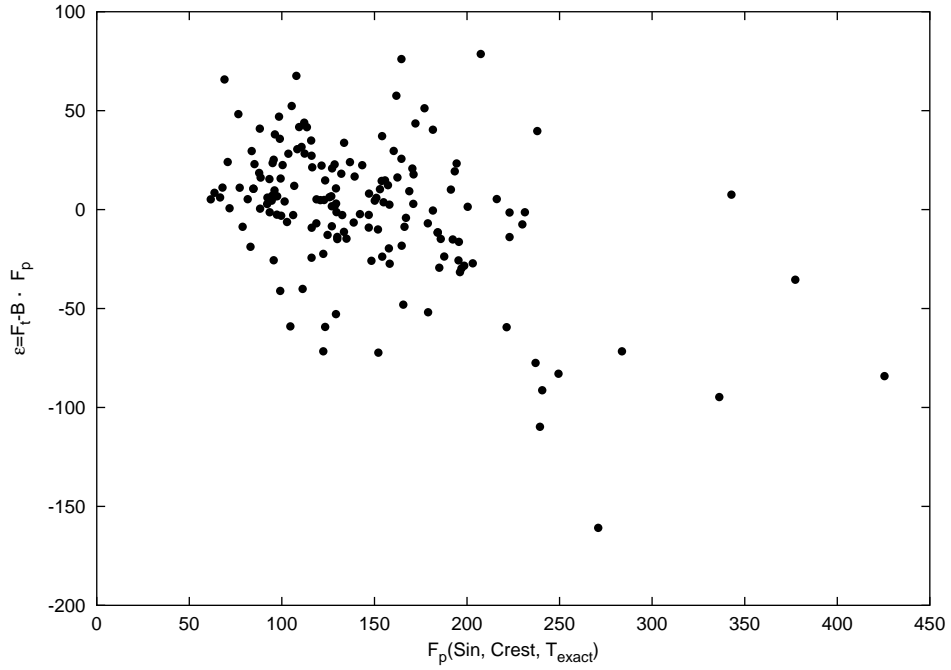


Figure 1: Comparing force prediction errors— ϵ from Eq. 2—with predicted forces F_p based on *crest heights*. Note negative correlation between ϵ and F_p .

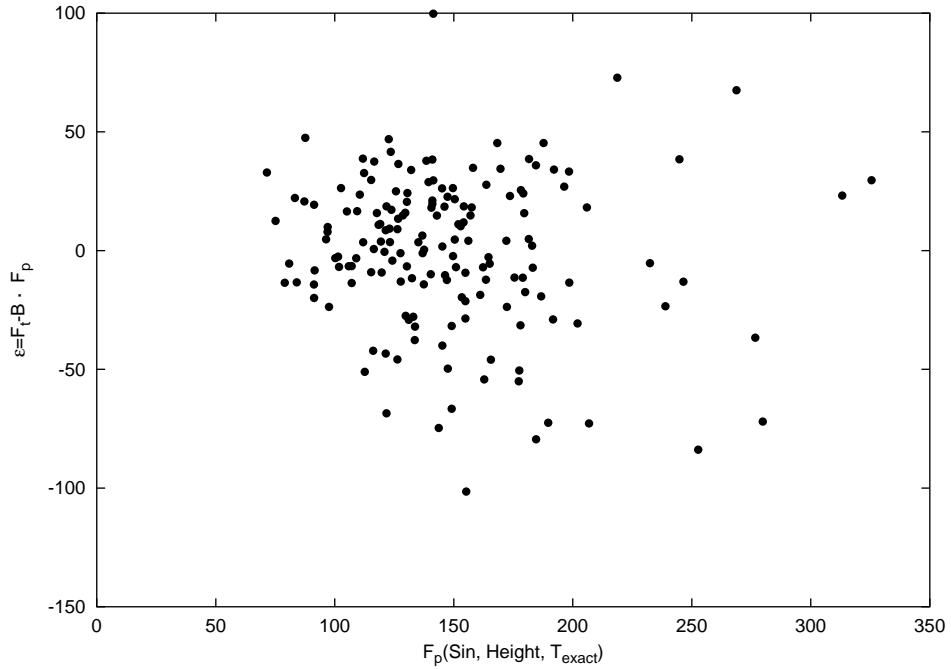


Figure 2: Comparing force prediction errors— ϵ from Eq. 2—with predicted forces F_p based on *wave heights*. As expected, little correlation is observed between ϵ and F_p .

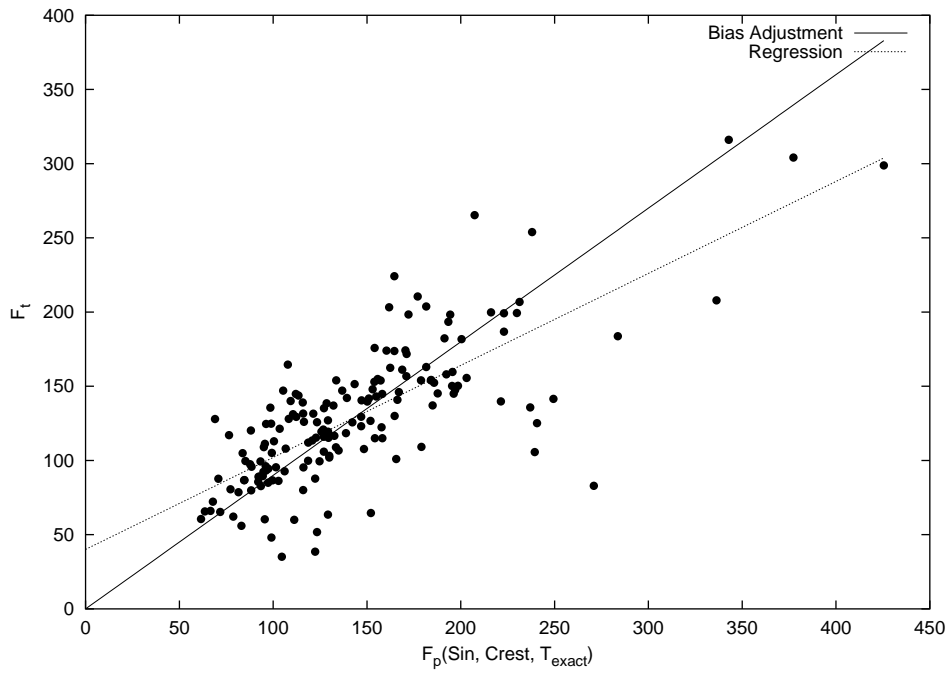


Figure 3: Comparing “true” forces F_t with predicted forces F_p based on *crest heights*.

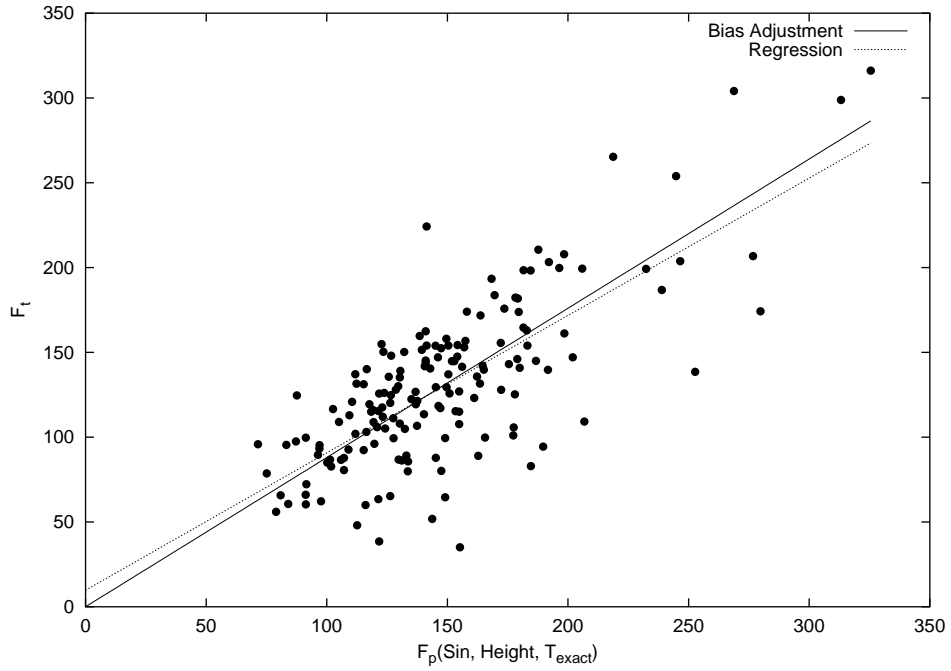


Figure 4: Comparing “true” forces F_t with predicted forces F_p based on *wave heights*.